

### USING 3D PRINTED LABYRINTHINE INCLUSIONS TO IMPROVE THE LOW-FREQUENCY PERFORMANCE OF A THIN, CONVENTIONAL SOUND-ABSORBING PANEL

### Michał Niedzielczyk Tomasz G. Zieliński\*

Institute of Fundamental Technological Research, Polish Academy of Sciences ul. Pawińskiego 5B, 02-106 Warsaw, Poland

#### **ABSTRACT**

The development of acoustic materials with broadspectrum efficiency remains a critical challenge, particularly for achieving effective low-frequency absorption. This study presents a composite sound absorber that combines a dense, conventional felt matrix with additively manufactured 3D printed inclusions designed to enhance low-frequency attenuation. These inclusions, fabricated using cost-effective Fused Filament Fabrication (FFF) technology, feature labyrinthine geometries with high tortuosity, designed to achieve subwavelength resonances. The combination of these elements results in a thin, lightweight, and scalable solution for sound attenuation. The design procedure developed for such composites is based on complex but fully analytical modelling. The composite material exhibits exceptional performance, achieving high levels of absorption at the designed low frequency due to inclusions, while maintaining efficient broadband characteristics of the matrix. The analytical predictions are confirmed experimentally by impedance tube measurements. By leveraging the advantages of additive manufacturing and conventional materials, this work paves the way for economically viable, tailored acoustic solutions.

**Keywords:** Acoustic composites, Conventional porous matrix, 3D printed labyrinthine inclusions, Multiscale modelling, Sound absorption.

\*Corresponding author: tzielins@ippt.pan.pl.

**Copyright:** ©2025 Michał Niedzielczyk and Tomasz G. Zieliński. This is an open-access article distributed under the terms of the Creative Commons Attribution 3.0 Unported License, which permits unrestricted use, distribution, and reproduction in any medium, provided the original author and source are credited.

#### 1. INTRODUCTION

Low-frequency sound absorption remains a major challenge in acoustic material design. Traditional porous absorbers, such as fibrous or foam-based materials, rely on viscous and thermal losses to dissipate acoustic energy [1]. While effective at mid-to-high frequencies, these materials require considerable thickness to achieve meaningful absorption at lower frequencies due to the inherent limitations of quarter-wavelength resonance. This constraint often conflicts with the practical need for thin, lightweight, and efficient sound absorbers, particularly in applications such as automotive interiors and aircraft structures.

To overcome this limitation, researchers have explored various approaches to enhance low-frequency sound absorption without excessively increasing material thickness. Acoustic metamaterials [2] have been developed to manipulate wave propagation in unconventional ways, enabling sub-wavelength sound absorption through engineered periodicity and resonance effects.

Many of these solutions are based on the use of resonant structures, such as Helmholtz resonators [3–5] of unconventional geometry, often in parallel arrangements, or micro-perforated panels [6,7] backed by air cavities of various shapes. The aim is to exploit resonance effects in order to improve acoustic absorption in specific low-frequency bands. Impedance-matching techniques [8–10] are used for graded or hierarchical structures to help transfer sound energy more effectively into dissipative regions. Another way to approach the problem is to extend the effective propagation path of sound waves in the volume of the material, thereby improving the energy dissipation mechanisms without a substantial increase in the material thickness. Solutions based on this idea include coiled-







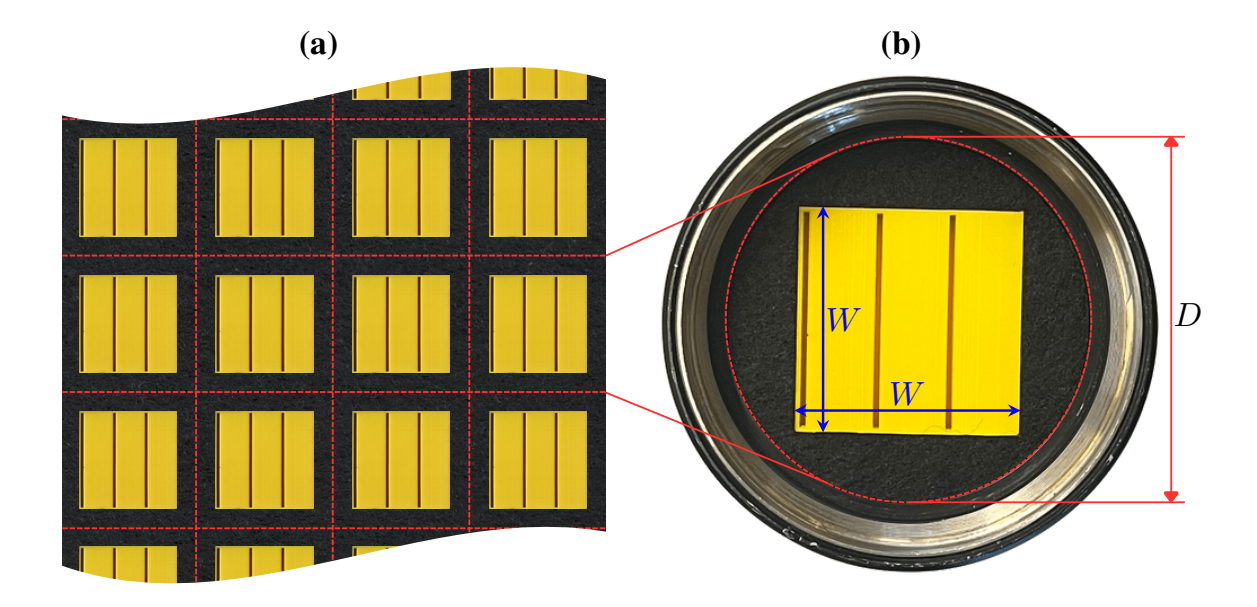


**Figure 1**. (a) Acoustic composite made of a black polyester felt panel with yellow 3D-printed inclusions embedded in a periodic arrangement; (b) sample of the composite panel inside a circular impedance tube.

up cavities and labyrinthine channels [11–14]. In parallel to the aforementioned strategies, the integration of engineered materials and metamaterials within composite absorbers [12, 15–17] has gained increasing attention. By embedding carefully tailored acoustic structures into conventional porous materials, it is possible to enhance energy dissipation mechanisms and extend the absorption to lower frequencies.

This study presents an experimentally validated analytical modelling of an acoustic composite to demonstrate how inexpensive and easy-to-3D-print inclusions can enhance the low-frequency sound absorption of conventional felt-based materials. The work addresses the above-mentioned critical limitation of traditional porous absorbers, which require significant thickness to achieve effective performance in the low frequency range.

The paper is structured as follows. Section 2 describes the composite material design and its components, including their fabrication and assembly. An acoustic modelling for predicting the performance of the composite absorber is discussed in Section 3. Section 4 discusses sound absorption results and provides experimental validation obtained through impedance tube measurements of a composite sample under normal incidence conditions. The key findings and conclusions are summarised in Section 5.

### 2. COMPOSITE PANEL

### 2.1 Design and components

Conventional polyester acoustic felt is known for its excellent sound absorption capacity in the mid- and high-frequency range. However, its relatively low tortuosity and high porosity limit its effectiveness at lower frequencies. To overcome this limitation, a composite structure is proposed in which labyrinthine metamaterial inclusions are embedded in a felt matrix.

Figure 1 (a) shows an example design of such a composite panel with a simple, periodic arrangement of identical inclusions. These inclusions have the shape of a cuboid with a square base and dimensions  $W \times W \times H$ , see Figure 2 (b) and Table 1 for the actual values of these and other dimensions. The inclusion thickness H is greater than the thickness  $H_F$  of the felt matrix, so an air gap is created behind the felt layer, which increases its absorption capacity. The proposed acoustic composite panel consists therefore of three materials: a conventional polyester felt, 3D-printed inclusions with labyrinthine channels, and air. The air fills the gap behind the felt layer, but also saturates the pores in the felt and the labyrinthine channels of the inclusions, thus acting as a medium for the propagation of sound waves.







Table 1. Useful dimensions (mm).

D	W	H	$H_{\mathrm{F}}$	$H_{G}$	w	a	b
63.5	40	18	9	9	1.05	0.8	6.35

An important aspect of designing the composite panel is determining the appropriate ratio of the inclusion surface area to the surface area of the felt matrix. This ratio plays an important role in the composite modelling, as discussed in Section 3. In this study, this proportion was adopted so that a composite sample that is representative of the entire composite panel could be tested in a circular impedance tube with an internal diameter of  $D=63.5 \, \mathrm{mm}$ , see Figure 1 (b).

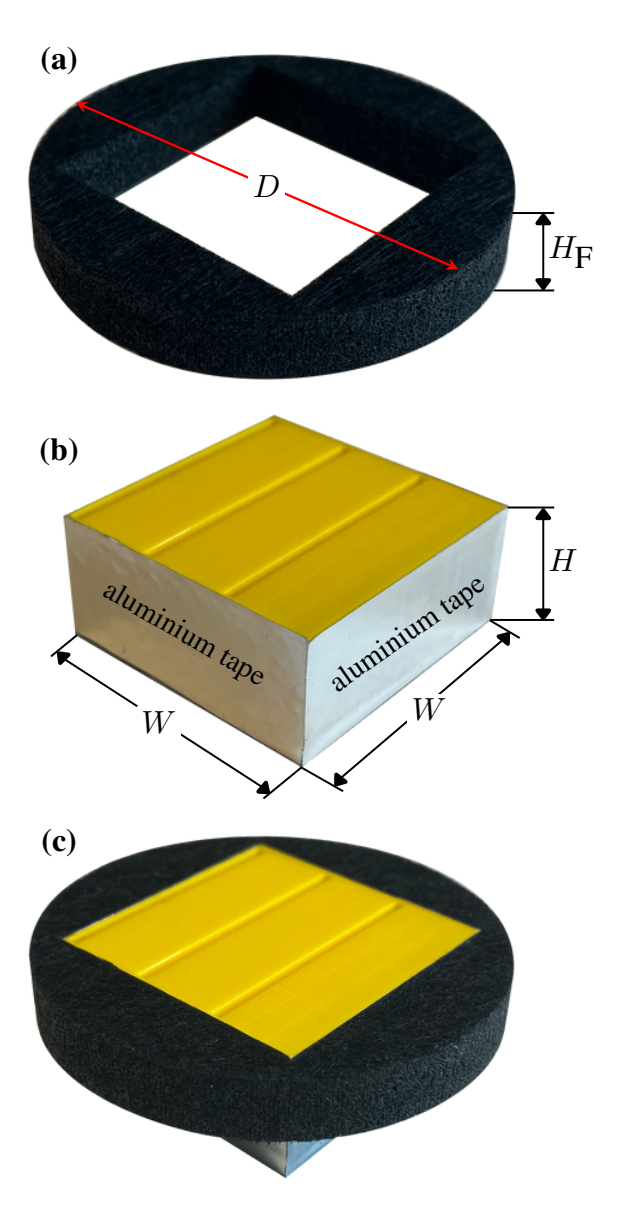
#### 2.2 Composite sample

Figure 2 shows two components, i.e. (a) the felt matrix and (b) the metamaterial inclusion, of a circular sample of the composite panel, as well as (c) the assembled sample ready for testing in a circular impedance tube. The component manufacturing and sample assembly procedure are described below.

A circular matrix sample of diameter D, see Figure 2 (b), was cut from the felt panel of thickness  $H_{\rm F}$ , using an optical laser cutter (Sculpfun S30 Pro Max). The cutting diameter was increased by the laser beam width of 0.3 mm. This dimensional compensation was applied to ensure precise fit of the sample inside the impedance tube. A similar compensation was applied when cutting the square hole with dimensions  $W \times W$  for the inclusion.

The labyrinthine inclusion shown in Figure 2 (b) was designed to contain three identical labyrinthine slits (channels) characterised by very high tortuosity, see Figure 3, and optimised for low-frequency sound absorption. It was additively manufactured from the thermoplastic polymer acrylonitrile-butadiene-styrene (ABS), which was selected for its reliability, quality and good mechanical properties. The two-dimensional inclusion design (see Figure 3) was optimised to facilitate efficient 3D-printing via Fused Filament Fabrication, taking into account in particular the size of the printing nozzle.

To ensure proper integration within the polyester felt matrix and eliminate acoustic leakage, aluminium tape was glued to the back and side surfaces of the inclusion as shown in Figure 2 (b). The taped inclusion was tightly fitted into the square hole of the felt matrix during assembly of the composite sample, Figure 2 (c).



**Figure 2**. (a) Matrix cut from a polyester felt panel; (b) 3D printed labyrinthine inclusion with the bottom and side surfaces covered with aluminium tape; (c) assembled composite sample.

### 3. ACOUSTIC MODELLING

### 3.1 Equivalent fluid approach

Acoustic modelling of the composite is based on the equivalent-fluid approach [1]. This means that both com-







**Table 2.** JCAL parameters for the composite panel components.

Material	φ (%)	$\alpha_{\infty}$ (-)	$\begin{array}{c} \Lambda_v \\ (10^{-6} \mathrm{m}) \end{array}$	$\begin{array}{c} \Lambda_{\text{th}} \\ (10^{-6}\text{m}) \end{array}$	$ \mathcal{K}_0 $ $ (10^{-10} \text{m}^2) $	$\Theta_0 $ $(10^{-10} \text{m}^2)$
polyester felt	96	1.1	27.3	82.5	3.21	5.89
labyrinth	52.43	38.02	1050	1050	12.67	481.7

ponents, i.e the felt material and the labyrinth inclusion, are modelled as effective acoustic fluids equivalent to rigid materials with open porosity saturated with air.

The well-known Johnson-Champoux-Allard-Lafarge (JCAL) model [1] is employed for both equivalent fluids. This model requires six intrinsic parameters of a porous material to fully describe its acoustic behaviour. These parameters are: porosity  $(\phi)$ , tortuosity  $(\alpha_{\infty})$ , viscous characteristic length  $(\Lambda_v)$ , thermal characteristic length  $(\Lambda_{th})$ , static viscous permeability  $(\mathcal{K}_0)$ , and static thermal permeability  $(\Theta_0)$ . They are discussed below for both composite components.

Once the six parameters are known for a porous material, its two dynamic permeabilities – viscous and thermal – can be calculated using the scaling functions of the JCAL model. The scaling functions, and therefore both dynamic permeabilities, depend on the frequency f. The dynamic viscous permeability also depends on the kinematic viscosity of the air saturating the pores, while the dynamic thermal permeability depends on the thermal diffusivity of air. The dynamic permeabilities are used to calculate the effective properties of the equivalent fluid: firstly, the effective density and compressibility, and then also the effective speed of sound and characteristic impedance. For this purpose, the ambient mean pressure and some other air properties are also required. Details can be found in Refs. [1, 18].

#### 3.2 Parameters for the conventional acoustic felt

For the acoustic polyester felt, the JCAL parameters were determined experimentally using inverse characterisation combined with gravimetric analysis. The Porosity was estimated directly by the gravimetric analysis, while the remaining five parameters were obtained by fitting theoretical predictions of the surface acoustic impedance and reflection coefficient to the corresponding experimental results measured in an impedance tube on a circular sample of the felt panel. This hybrid procedure ensured correct parameter estimation, enabling precise modelling of

the acoustic behaviour of the felt. The parameters characterised for the felt material are given in Table 2.

#### 3.3 Parameters for the labyrinthine inclusion

In contrast to the felt, all six JCAL parameters can be determined analytically for the 3D printed labyrinthine inclusion, because its microstructural geometry is relatively simple and well-defined. It is clearly visible in Figure 3 which shows a cross-section of the composite sample. The inclusion has three identical labyrinthine channels of constant width w, which along with the remaining two dimensions a and b (see Figure 3) uniquely define the two-dimensional microgeometry of the inclusion. The actual values of all necessary dimensions are given in Table 1. These dimensions allow for a direct calculation or estimation of the required JCAL parameters.

The porosity defined as the volume ratio of air in the three channels to the total volume of the inclusion can be determined from the microstructural geometry of its cross-section (see Figure 3), namely

$$\phi = \frac{3w\ell}{WH} \,, \tag{1}$$

where

$$\ell = 16a + 14b + 14w \tag{2}$$

is the length of each labyrinthine channel (calculated along its centreline with sharp corners at each bend).

Since the channels are identical and have a constant width, the kinematic tortuosity can be estimated using the definition of geometric tortuosity [13, 19, 20], i.e. as the squared ratio of the channel length  $\ell$  to the material thickness H. Zielinski et al. [13] demonstrated that to make this estimation more accurate the channel length should be replaced by the estimated length of the flow path through the channel

$$\widetilde{\ell} \approx \ell - 24w + 24\frac{\pi}{2}\frac{w}{2}.$$
 (3)

Here, the flow path is accurately approximated by the channel centreline with rounded corners (at each of







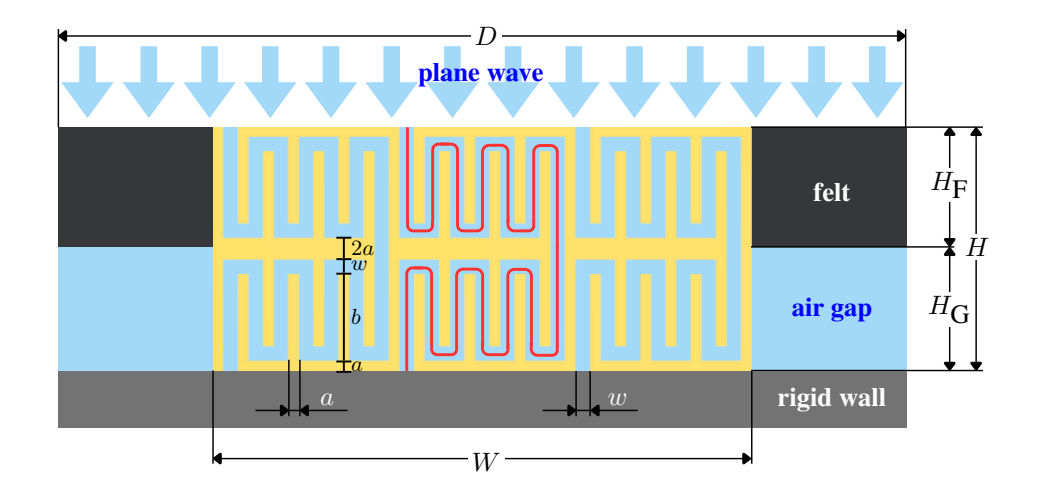


**Figure 3**. Cross-section of the composite panel (see Table 1 for the actual dimensions).

24 bends), marked with a red curve in Figure 3. Therefore, the tortuosity of the labyrinthine material is calculated as follows

$$\alpha_{\infty} \approx (\widetilde{\ell}/H)^2$$
. (4)

For a channel with constant width, the thermal characteristic length is equal to its width. This also applies to the characteristic viscous length if the channel is straight. When it is tortuous, as in the case of labyrinthine slits of this work, the channel width is still a very good approximation of the viscous length [1, 13]. Therefore,

$$\Lambda_{\rm v} \approx \Lambda_{\rm th} = w$$
 (5)

Based on the determined parameters, the viscous and static thermal permeabilities can be computed for the material with labyrinthine slits, using the following formulae

$$\mathcal{K}_0 \approx \frac{\phi w^2}{12\alpha_{\infty}}, \qquad \Theta_0 \approx \frac{\phi w^2}{12}.$$
 (6)

The values of JCAL parameters calculated for the labyrinthine inclusion are listed in Table 2, where they can be confronted with those determined for the felt material.

#### 3.4 Surface acoustic impedances

The JCAL parameters determined for the felt matrix and labyrinth inclusion (see Table 2) allowed the calculation of the effective properties for both equivalent fluids that represent these materials in acoustic modelling. In particular, the effective speed of sound for the felt material  $c_{\rm F}$ 

and for the labyrinth  $c_{\rm L}$  were calculated along with the corresponding characteristic impedances,  $Z_{\rm F}$  and  $Z_{\rm L}$ , respectively. Recall that all these effective properties are complex functions of frequency.

The effective properties can be used to determine sound wave propagation in fluids equivalent to porous materials. Important acoustic indicators such as surface acoustic impedance of a porous layer can be determined. The surface acoustic impedance  $\mathcal{Z}_{\rm sF}$  of a hard-backed felt panel with thickness  $H_{\rm F}$  and the surface impedance  $\mathcal{Z}_{\rm sL}$  of a hard-backed labyrinthine material with thickness  $H_{\rm L}$  are calculated as follows

$$\mathcal{Z}_{\rm sF} = Z_{\rm F} \coth(\mathrm{i}\omega H_{\rm F}/c_{\rm F}), \qquad (7)$$

$$\mathcal{Z}_{\text{SL}} = Z_{\text{L}} \coth(\mathrm{i}\omega H/c_{\text{L}})$$
 (8)

Here,  $\omega = 2\pi f$  is the angular frequency and  $i = \sqrt{-1}$ .

Recall that the felt matrix in the composite panel is backed by an air gap of thickness  $H_{\rm G}=H-H_{\rm F}$ , see Figure 3. Therefore, the surface acoustic impedance of such a two-layer system is required, i.e.

$$\mathcal{Z}_{sFG} = \frac{\mathcal{Z}_{sF}^2 + \mathcal{Z}_{sF} \mathcal{Z}_{sG}}{\mathcal{Z}_{sF} + \mathcal{Z}_{sG}}.$$
 (9)

In the formula above

$$\mathcal{Z}_{sG} = Z_0 \coth(i\omega H_G/c_0)$$
 (10)

is the surface acoustic impedance of a hard-backed air gap with thickness  $H_{\rm G}$ . Here,  $Z_0$  and  $c_0$  are the characteristic impedance and speed of sound in air, respectively.







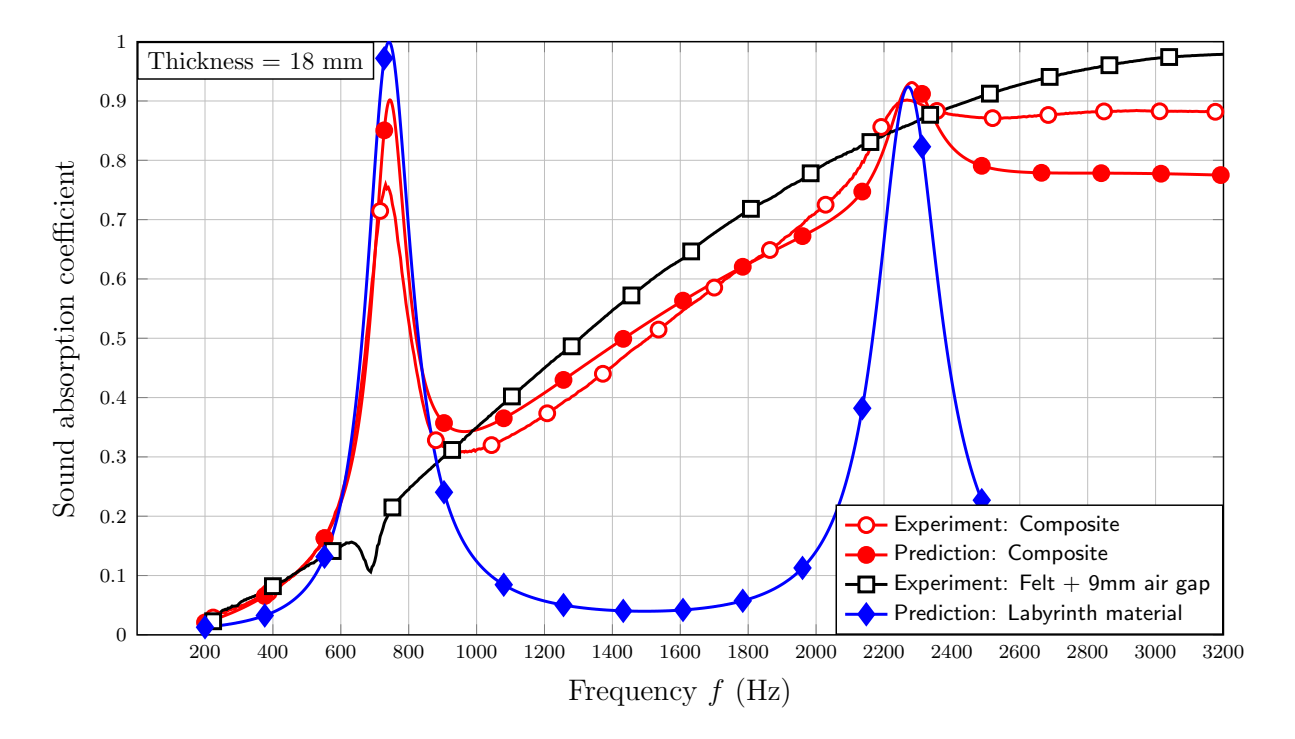


**Figure 4**. Sound absorption measured and predicted for the acoustic composite sample, measured for the felt panel backed by an air gap, and calculated for the labyrinthine material.

Finally, the surface acoustic impedance of the composite panel can be determined as

$$\mathcal{Z}_{sC} = \frac{1}{\Phi_L/\mathcal{Z}_{sL} + (1 - \Phi_L)/\mathcal{Z}_{sFG}}, \qquad (11)$$

where

$$\Phi_{\rm L} = \frac{W^2}{\pi D^2/4} \tag{12}$$

is the fraction of the inclusion face area relative to the front surface area of the composite sample, see Figure 1 (b). Formula (11) describes in fact the combined surface acoustic impedance of two components, i.e. the air-supported felt matrix and the labyrinthine inclusion arranged (acting) in parallel [21].

#### 4. SOUND ABSORPTION

#### 4.1 Predictions and measurements

This section presents the predictions and measurement results of sound absorption at normal incidence for the acoustic composite studied in this work. The predictions were calculated using the surface acoustic impedances defined in Section 3.4 and the well-known formulae for the reflection and sound absorption coefficients, see e.g. Ref. [1]. The experimental measurements were performed on the composite sample, see Figure 1 (c), using an impedance tube set-up according to ISO standard 10534-2 [22]. The impedance tube has an internal diameter of D=63.5 mm, which ensures plane wave propagation within the frequency range of interest up to 3.2 kHz. The transfer function method with two microphones was used to determine the sound absorption coefficient under normal incidence conditions [22].

Figure 4 shows both the experimental and analytical results obtained for the composite sample. A prediction of sound absorption for the labyrinthine material itself is also presented, as well as the absorption curve measured for the homogenous felt panel backed by an air gap.

#### 4.2 Comparison and discussion of the results

The sound absorption curves shown in Figure 4 can be compared, as they all correspond to configurations with the same total thickness of  $H=18\,\mathrm{mm}$ .







The black curve with square markers represents the absorption coefficient measured for a reference configuration consisting of a 9 mm polyester felt backed by a 9 mm air gap. As expected, this material exhibits very good absorption capacity in the mid- and high-frequency ranges, but rather poor performance at lower frequencies, although the overall absorption is improved by the air gap. Furthermore, the undesirable effect related to the resonance of the elastic skeleton of the felt is clearly visible around 700 Hz. It locally reduces the already weak low-frequency absorption. Incidentally, such poroelastic behaviour occurs only around this resonant frequency of the skeleton, and the rigid-frame equivalent-fluid model is appropriate and valid for the entire frequency range beyond the elastic-skeleton resonance.

To overcome the limitations of the felt acoustic panel, a labyrinth inclusion was designed using the model described in Section 3 to introduce a subwavelength resonance with a frequency similar to the resonance frequency of the elastic skeleton of the felt. This is evidenced by the corresponding sound absorption calculated for the labyrinthine material, represented with the blue curve with diamond markers in Figure 4. This curve has two absorption peaks and perfect absorption is achieved with the first peak at about 750 Hz.

After embedding the labyrinthine inclusion in the polyester felt to form an acoustic composite panel, significant improvement in sound absorption was achieved in the targeted low frequency range. The predicted and measured acoustic absorption performance of the composite is shown in Figure 4 by two red curves marked with circles. These curves show good agreement with each other, which confirms the validity of the analytical model proposed in Section 3. It is easy to observe that incorporating the labyrinthine inclusion into the polyester felt does not degrade its good mid-to-high-frequency sound absorption. Instead, the combined acoustic absorption performance of a conventional porous matrix and a metamaterial inclusion is achieved.

#### 5. CONCLUSIONS

An acoustic composite panel combining conventional acoustic felt with 3D-printed labyrinthine inclusions was researched and designed to enhance low-frequency sound absorption while retaining the natural ability of the felt to absorb mid- and high-frequency noise.

The impedance-tube measurements performed on a composite sample confirm that tailored labyrinthine in-

clusions can significantly increase the sound absorption at low frequencies through a quarter-wavelength resonance tuned in design. At the same time, embedding metamaterial inclusions into the felt matrix in the appropriate proportion does not significantly affect the good performance of the matrix material in the mid and high frequency range, offering a lightweight and space-saving solution for broadband sound absorption.

The good agreement of the measurement results with the predictions proved that the applied analytical modelling based on the equivalent fluid approach and the calculation of the surface impedance of the sound-absorbing elements working in parallel are correct and accurate.

Future work will focus on manufacturing larger composite samples and testing them in different configurations and noise conditions, e.g. as liners in a duct or in a diffuse field, to evaluate their performance under real-world conditions.

#### 6. ACKNOWLEDGMENTS

This research was financially supported by the National Science Centre (NCN), Poland, under Grant Agreement No. 2021/41/B/ST8/04492.

#### 7. REFERENCES

- [1] J. F. Allard and N. Atalla, *Propagation of Sound in Porous Media: Modeling Sound Absorbing Materials, 2nd ed.* Chichester: John Wiley & Sons, 2009.
- [2] J.-P. Groby, N. Jiménez, and V. Romero-García, "Acoustic metamaterial absorbers," in *Acoustic Waves* in *Periodic Structures, Metamaterials, and Porous Media: From Fundamentals to Industrial Applications* (N. Jiménez, O. Umnova, and J.-P. Groby, eds.), ch. 5, pp. 167–204, Cham: Springer International Publishing, 2021.
- [3] J. Huang, J. Wang, T. Ma, H. Wei, S. Zhang, G. Wang, L. Wang, Q. Wang, W. Zhou, and Z. Zhang, "Composite structure with porous material and parallel resonators for broadband sound absorption at low-to-mid frequencies," *Applied Acoustics*, vol. 225, p. 110193, 2024.
- [4] W. Kong and T. Fu, "A novel butterfly double-panel metastructure filled with porous materials for broadband low-frequency sound absorption," *Journal of Building Engineering*, vol. 97, p. 110935, 2024.







- [5] S. Bi, E. Wang, X. Shen, F. Yang, X. Zhang, X. Yang, Q. Yin, C. Shen, M. Xu, and J. Wan, "Enhancement of sound absorption performance of Helmholtz resonators by space division and chamber grouping," *Applied Acoustics*, vol. 207, p. 109352, 2023.
- [6] Y. Qian, B. Li, and J. Zhang, "Study of ultra-wideband acoustic metamaterial based on multi-order broadband resonance band coupling of ultra-micro perforated panel," *Applied Acoustics*, vol. 235, p. 110643, 2025
- [7] P.-F. Zhang, Z.-H. Li, Y.-J. Zhou, Q.-F. Zhang, B. Liu, F. Liu, S.-C. Pei, K. Shi, and P. kang Bai, "Improved sound absorption with 3D-printed micro-perforated sandwich structures," *Journal of Materials Research and Technology*, vol. 34, pp. 855–865, 2025.
- [8] F. Wu, X. Zhang, Z. Ju, J. Zhao, M. Hu, M. Gao, J. Luo, and H. Pu, "Ultra-broadband sound absorbing materials based on periodic gradient impedance matching," *Frontiers in Materials*, vol. 9, 2022.
- [9] Y. Liu, X. Zeng, S. Ren, W. Sun, H. Wang, and Y. Lei, "A broadband multi-resonant sound-absorbing metastructure based on impedance-matching nesting channels," *Applied Acoustics*, vol. 223, p. 110099, 2024.
- [10] S. Ren, Y. Liu, W. Sun, H. Wang, Y. Lei, H. Wang, and X. Zeng, "Broadband low-frequency sound absorbing metastructures composed of impedance matching coiled-up cavity and porous materials," *Applied Acoustics*, vol. 200, p. 109061, 2022.
- [11] G. do N. Almeida, E. F. Vergara, L. R. Barbosa, A. Lenzi, and R. S. Birch, "Sound absorption metasurface with symmetrical coiled spaces and micro slit of variable depth," *Applied Acoustics*, vol. 183, p. 108312, 2021.
- [12] H. Zhao, Y. Wang, D. Yu, H. Yang, J. Zhong, F. Wu, and J. Wen, "A double porosity material for low frequency sound absorption," *Composite Structures*, vol. 239, p. 111978, 2020.
- [13] T. G. Zieliński, K. C. Opiela, N. Dauchez, T. Boutin, M.-A. Galland, and K. Attenborough, "Extremely tortuous sound absorbers with labyrinthine channels in non-porous and microporous solid skeletons," *Applied Acoustics*, vol. 217, p. 109816, 2024.
- [14] I. Lee, I. Han, and G. Yoon, "Compact acoustic metamaterials based on azimuthal labyrinthine channels for broadband low-frequency soundproofing and

- ventilation," Applied Acoustics, vol. 228, p. 110273, 2025.
- [15] C. Lagarrigue, J. P. Groby, V. Tournat, O. Dazel, and O. Umnova, "Absorption of sound by porous layers with embedded periodic arrays of resonant inclusions," *The Journal of the Acoustical Society of America*, vol. 134, pp. 4670–4680, 12 2013.
- [16] Y. Fang, X. Zhang, J. Zhou, J. Guo, and X. Huang, "Acoustic metaporous layer with composite structures for perfect and quasi-omnidirectional sound absorption," *Composite Structures*, vol. 223, p. 110948, 2019.
- [17] Q. Xu, J. Qiao, Z. Ren, J. Sun, G. Zhang, and L. Li, "Multi synergistic coupling design for broadband sound absorption based on compact porous composite embedded with massless membrane resonator," *Composite Structures*, vol. 286, p. 115312, 2022.
- [18] T. G. Zieliński, R. Venegas, C. Perrot, M. Červenka, F. Chevillotte, and K. Attenborough, "Benchmarks for microstructure-based modelling of sound absorbing rigid-frame porous media," *Journal of Sound and Vibration*, vol. 483, p. 115441, 2020.
- [19] K. Attenborough, "Microstructures for lowering the quarter wavelength resonance frequency of a hard-backed rigid-porous layer," *Applied Acoustics*, vol. 130, pp. 188–194, 2018.
- [20] B. Ghanbarian, A. G. Hunt, R. P. Ewing, and M. Sahimi, "Tortuosity in porous media: A critical review," *Soil Science Society of America Journal*, vol. 77, no. 5, pp. 1461–1477, 2013.
- [21] K. Verdière, R. Panneton, S. Elkoun, T. Dupont, and P. Leclaire, "Transfer matrix method applied to the parallel assembly of sound absorbing materials," *The Journal of the Acoustical Society of America*, vol. 134, pp. 4648–4658, 12 2013.
- [22] "ISO 10534-2: Determination of sound absorption coefficient and impedance in impedance tubes," 1998.



